Research Square

Preprints are preliminary reports that have not undergone peer review.
They should not be considered conclusive, used to inform clinical practice,
or referenced by the media as validated information.

# Influence of Train Speed on Ground Surface Vibrations in Urban Rail Tunnels

**Sakineh Etemadi**
Tarbiat Modares University
**Soheil Sharifi Boroujerdi**
sharifi.s@modares.ac.ir
Tarbiat Modares University
**Hamid Reza Nejati**
Tarbiat Modares University
**Seyed Amin Moosavi**
Vali-e-Asr University of Rafsanjan
**Reza Nateghi**
Tarbiat Modares University
**Kamran Goshtasbi**
Tarbiat Modares University
**Masoud Abedini**
Shenyang University of Technology

**Article**

**Keywords:** Train Dynamic Load, Ground-Borne Vibration, Numerical Modeling, Dynamic Analysis

**Posted Date:** July 27th, 2026

**DOI:** https://doi.org/10.21203/rs.3.rs-10138140/v1

**License:** This work is licensed under a Creative Commons Attribution 4.0 International License.
Read Full License

**Additional Declarations:** No competing interests reported.

# Influence of Train Speed on Ground Surface Vibrations in Urban Rail Tunnels

Sakineh Etemadi[1], Soheil Sharifi Boroujerdi [*1], Hamidreza Nejati[1], Seyed Amin Moosavi[2], Reza Nateghi[1], Kamran Goshtasbi[1], Masoud Abedini[3]

1. Rock Mechanics Division, School of Engineering, Tarbiat Modares University, Tehran, Iran.
2. Mining Engineering Department, Vali-e-Asr University of Rafsanjan, Rafsanjan, Iran
3. Multidisciplinary Center for Infrastructure Engineering, Shenyang University of Technology, Shenyang 110870, China

Corresponding author: Soheil Sharifi Boroujerdi

**Abstract**

As underground rail networks expand, train-induced vibrations increasingly affect nearby structures, disturbing residents and sensitive equipment. One of the critical aspects of this research is the investigation of ground vibrations induced by train movements within tunnels. To address this issue, Line 6 of the Tehran Metro has been selected as a case study. A numerical approach was employed to simulate the dynamic loads exerted by trains operating at various speeds. The modeling process was conducted in two phases using finite element analysis. First, the dynamic loads resulting from wheel–rail interaction were determined. Then, the finite element method was applied to evaluate the ground vibration levels caused by underground train movements. Vibration velocity levels were analyzed at train speeds of 40, 60, and 90 kilometers per hour. Given the double-track configuration of the Tehran Metro, nine distinct scenarios were considered. The results reveal that the scenario involving the simultaneous movement of two trains at 90 km/h produces the highest ground surface vibrations. The vibration velocity level in this case reaches 84 decibels, which may be disruptive to nearby residents. Overall, the findings indicate that increasing train speed leads to higher peak particle velocities, thereby intensifying ground vibration levels.

**Key words**: Train Dynamic Load, Ground-Borne Vibration, Numerical Modeling, Dynamic Analysis

## 1. Introduction

With the continued development and expansion of underground railway networks, coupled with increasing train speeds, environmental concerns related to vibrations induced by train movements have garnered significant attention. These vibrations frequently disrupt residential areas and pose potential risks to surface structures and sensitive equipment (Gardien & Stuit, 2003). Train movement generates time-dependent dynamic loads that are transmitted from the wheel to the rail, then propagated through the track structure to the subgrade and surrounding ground. The dynamic characteristics of these loads, particularly in high-speed railway systems, play a critical role in

* Corresponding Author
Email Address: sharifi.s@modares.ac.ir
Tel: +982182883380

shaping the overall vibrational behavior of the track infrastructure. Generally, train-induced loads are categorized into three primary components: vertical, longitudinal, and lateral. Among these, vertical loads, arising from the interaction between the wheel and the track's vertical reaction, are typically manifested as upward pressure (Indraratna et al., 2011; Ahmadi el al., 2012). Given their dominant influence on ground vibration transmission, this study focuses exclusively on vertical loads. The vertical loads exerted by trains on the track structure, crucial for the design of railway subgrades, can be classified into four categories: static, quasi-static, impact, and dynamic loads. Among these, dynamic loads play a pivotal role in the interaction between moving trains and the track system. These loads are influenced by several variables, including axle spacing, axle weight, and train speed. Collectively, these factors serve as primary determinants of ground vibration levels. In addition to these, various secondary sources also contribute to the vibrational response of the track structure (Hall, 2003; Nejati et al., 2012).

### 1.1 Evaluating Dynamic Loads in Trains

The study of loads generated by train movement encompasses experimental methods, laboratory and field measurements, as well as analytical and numerical approaches. Experimental design for railway tracks involves identifying the loads acting on structural components and subsequently developing a stable track system capable of withstanding these forces. However, this method is limited by the narrow range of parameters considered and the reliance on design criteria that often result in conservative estimations. Accounting for the dynamic effects of loads is essential in railway track design, yet accurately predicting these loads remains a significant challenge. To address this, the load exerted by train wheels is typically multiplied by a factor known as the Dynamic Amplification Factor (DAF), which compensates for internal dynamic effects within the track structure. Foundational research in this area includes studies by Deutsche Bahn (Doyle, 1980), Sadeghi and Barati (2010), Dung et al. (2020), and the Union Internationale des Chemins de Fer (UIC 713R, 2004). Additionally, Naude (2006) employed both laboratory and field measurements to quantify vertical and lateral loads during train passage. Dynamic analysis of railway tracks is typically initiated through analytical modeling, followed by evaluation of the system's dynamic response. These equations are then solved using numerical methods to determine the magnitude and impact of train-induced loads on the subgrade. Notable analytical studies include those by Xu et al. (2015), Sadeghi et al. (2016), Jin (2016), Aggestam et al. (2018), Ling et al. (2020), Zhu et al. (2020), Jiang et al. (2020), Qu et al. (2020), Vale (2021), and Li et al. (2021). Numerical methods, particularly finite element modeling (FEM), offer a robust framework for simulating the physical behavior of train wheels, rails, tracks, and subgrades under realistic geometrical and loading conditions. For instance, Ntotsios et al. (2019) modeled train-induced vibrations in both ballasted and non-ballasted tracks, while Heidary et al. (2021) investigated the influence of train speed on ground surface vibrations in twin tunnels. Qu et al. (2021) conducted a comprehensive study on vibration source characteristics and propagation dynamics, and Faizan et al. (2022) validated high-speed train vibration models through field measurements.

Further contributions include Huang et al. (2017), who developed a rail-fastener-tunnel-subgrade model and extended it to 3D subway train simulations; Forde et al. (2017), who analyzed slab track dynamics using 2D FEM; Wang et al. (2020), who employed MIDAS software to assess tunnel lining responses; and Dai et al. (2021), who used Abaqus for 3D vibration analysis in subway tunnels. Wu et al. (2021) applied a 2D discrete element model to compare vibration responses in

tunnels of varying diameters, while Li et al. (2021) examined the dynamic interaction between subway trains and adjacent tunnel structures using Abaqus. Among the available methodologies, analytical and numerical approaches, particularly those grounded in FEM, are recognized as the most precise and reliable for evaluating train-induced dynamic loads. Accordingly, this study employs numerical analysis to investigate the dynamic loads generated by train movement.

## 2. Research methodology

### 2.1 Train dynamic load

Several techniques are available for predicting vibrations induced by passing trains. This research employs a numerical approach to evaluate ground surface vibrations resulting from underground train movements. The study begins by simulating the dynamic loads generated at the wheel–track interface using the finite element method (FEM). These calculated loads, corresponding to specific train speeds, are subsequently used to model the vibration response of the surrounding ground.

For simulating the train–slab track–subgrade system, a three-dimensional numerical model was developed. The model includes representations of the train wheel and rail, while the carriage and suspension systems are incorporated as equivalent components. In modeling the track and subgrade system, only the rail is explicitly represented; the rail fasteners, concrete slab tracks, and track foundation are simplified as equivalent structural elements.

The geometry of the train wheel follows the S1002 cross-sectional profile Fig. 1(a), and the UIC54E1 track geometry is adopted for rail modeling Fig. 1(b). An elastic material behavior is assumed for both the wheel and rail components, with careful consideration given to contact mechanics, stress limitations, and the mechanical properties of steel under dynamic loading conditions. The input parameters used in each section of the model are summarized in Table 1.

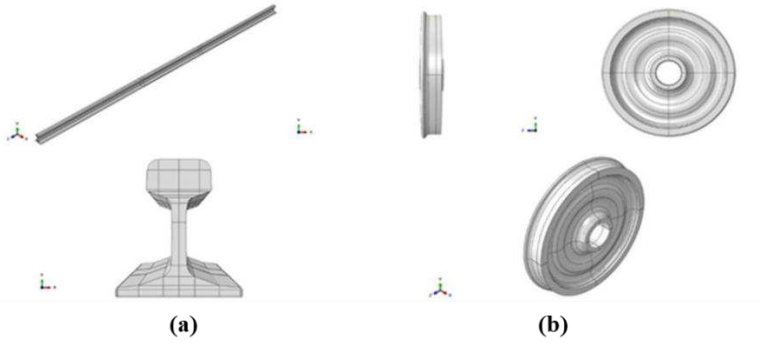



Fig. 1. (a) S1002 cross-section profile (b) UIC54E1 track geometry

Table 1. Input parameters for the modeling in each section

| Input parameter | wheel | rail |
|---|---|---|
| Density (kg/m³) | 7800 | 7800 |
| Elastic modulus (Pa) | $205 \times 10^9$ | $210 \times 10^9$ |
| Poisson's ratio | 0.3 | 0.29 |

In this study, the passage of a train wagon is used as the basis for determining dynamic loads, with particular emphasis on the vibrations generated by train movement. Since lower train speeds result in longer travel durations over a fixed distance, a speed of 40 km/h is selected as the baseline for analysis. The train wagon, consisting of eight wheels distributed across four axles, serves as the reference unit for length, with 40 km/h representing the slowest of the three evaluated speeds.

To assess the effects of higher speeds, specifically 60 and 90 km/h, the time required to traverse the same distance at the baseline speed is used as a reference. The corresponding length, equivalent to the car body length, is adopted as the comparative unit for analysis across all speeds.

The dynamic load derived from numerical modeling at each speed pertains to a single wheel axle. To capture the output of dynamic loads resulting from wheel–rail contact, two solution areas were defined on the contact surface, spaced 1.5 meters apart—equivalent to the distance between two adjacent train wheels. The length of each solution area is determined based on the train's speed, ensuring that the rail distance covered at each speed corresponds to equal time intervals. As the train wheel traverses these solution areas, dynamic load outputs are recorded.

Fig. 2 illustrates one of the designated solution areas, while Table 2 presents the corresponding length dimensions for each train speed.

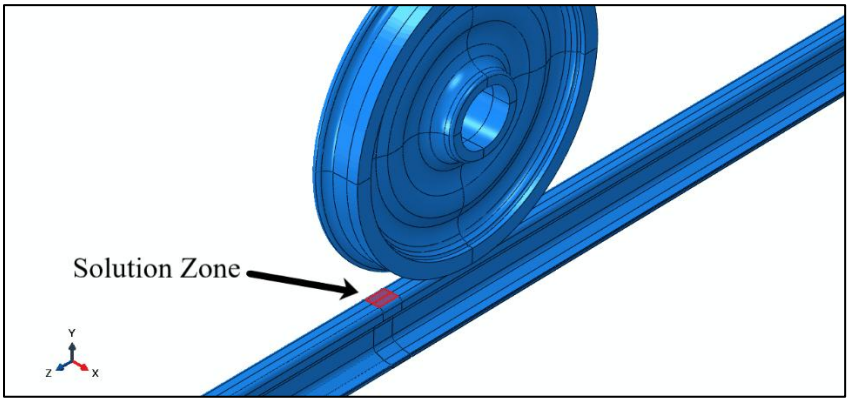



Fig. 2. Solution area

Table 2. Dimensions of the solution area for recording dynamic load

| Speed ($^{km}/_{h}$) | length dimension of solution area (m) | Time (s) |
|---|---|---|
| 40 | 0.044 | 0.004 |
| 60 | 0.067 | 0.004 |
| 90 | 0.1 | 0.004 |

Following the initial positioning of the wheel on the rail, surface-to-surface contact is explicitly defined using the penalty contact method to ensure continuous interaction between the wheel and track throughout the simulation. The contact properties are divided into two components: vertical behavior, modeled as hard contact, and tangential behavior, characterized by a friction coefficient of 0.3.

The equations governing the wheel component incorporate the axle weight, wagon mass, and the primary suspension system. To represent the combined effect of the train wheel and suspension system, a Multiple Point Constraint (MPC) is applied. This constraint links the motion of all selected nodes to a single reference point. In this model, the motion of all nodes on the inner surface of the wheel's central hole—where the wheel is mounted on the axle—is constrained to reference point RP-1, located at the center of the hole. Half of the axle weight is applied as a lumped mass at RP-1.

The primary suspension system is modeled using spring-damper elements and is incorporated at reference point RP-2, as illustrated in Fig. 3. At RP-2, the mass of the car body, bogies, and passengers is represented as an equivalent lumped load. For the rail section, equivalent components include the rail pad and subgrade, encompassing sleepers, rail fasteners, and concrete slab tracks.

To model sleeper behavior, as shown in Fig. 4, spring-damper elements are assigned to each sleeper. These are distributed over a 6-meter rail segment, with eight sleepers spaced at 0.75-meter center-to-center intervals and each sleeper having a length of 0.27 meters.

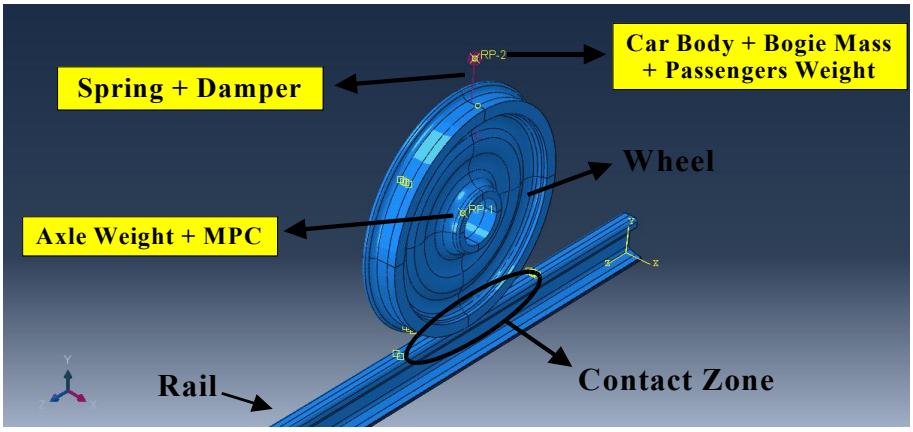



Fig. 3. Equivalences applied to the wheel

To simulate the interaction between the rail and subgrade, eight reference points (RP3 to RP10) located at the center of the sleepers are tied to corresponding nodes on the underside of the rail using Multiple Point Constraints (MPC). Additionally, eight reference points positioned beneath the sleepers (RP11 to RP18) are introduced to represent the track bed and ensure structural equilibrium.

Table 3 presents the mechanical properties of the spring-damper components used to model the sleeper–subgrade interaction. It also includes the weight parameters for the wheel axle, lumped

mass, car body, bogie assembly, and passenger load, all of which are incorporated into the simulation as equivalent masses.

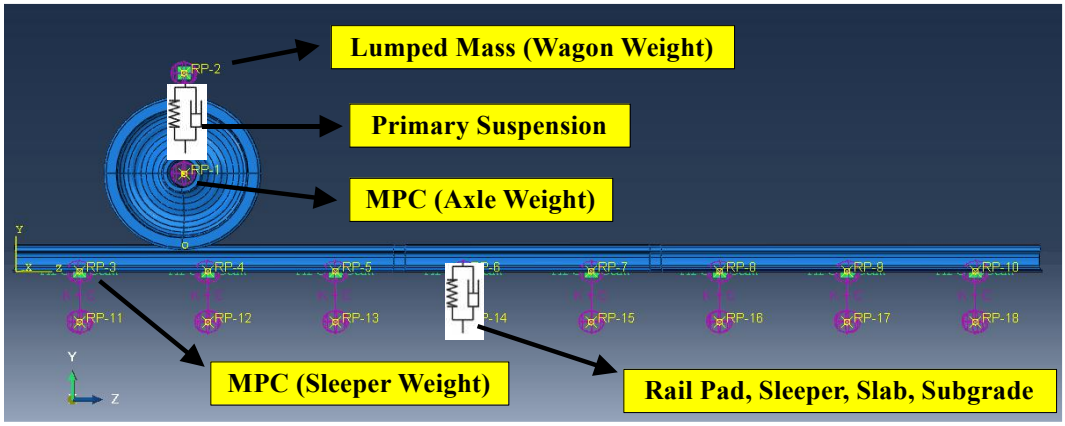



Fig. 4. Schematic representation of the equations

The dynamic load exerted by the train was simulated at speeds of 40, 60, and 90 km/h, and the corresponding load values were calculated for each case. As illustrated in Fig. 5, the maximum dynamic loads recorded at 40, 60, and 90 km/h are 147.7 kN, 178.9 kN, and 214.4 kN, respectively. With increasing train speed, the load profiles exhibit greater fluctuations, indicating more pronounced dynamic effects. For this study, the wagon shown in Fig. 6, featuring eight wheels distributed across four axles, is used as the reference unit for base length. The dynamic load obtained from numerical modeling at each speed corresponds to a single wheel axle. Assuming uniform load distribution across all wheels, the final dynamic load associated with each speed and base length was determined.

At a speed of 40 km/h, the base length is traversed in approximately 1.9 seconds, corresponding to the passage of four wheel axles. The cumulative dynamic load for this condition is presented in Fig. 7(a). For speeds of 60 and 90 km/h, the final dynamic loads were calculated based on equal time intervals to ensure consistent comparison across all three speeds. As shown in Fig. 7(b), at 60 km/h the train travels a distance of 31.564 meters, equivalent to six wheel axles. At 90 km/h, the distance covered is 47.5 meters, corresponding to eight wheel axles, as depicted in Fig. 7(c).

Table 3. Properties of the spring-damper components

| Component | properties |
|---|---|
| weight of the car body, bogies mass and passengers weight For each individual wheel | 9100 kg |
| axle weight (RP-1) | 238 kg |
| spring-damper (RP-2) | Stiffness $2.08 \times 10^6$ N/m |
| spring-damper (RP-2) | damping coefficient $1 \times 10^5$ N·s/m |
| Lumped mass (PR3 – PR11) | 150 kg |
| spring-damper (PR3 – PR10) | Stiffness $2.9 \times 10^9$ N/m |
| spring-damper (PR3 – PR10) | damping coefficient $2.207 \times 10^5$ N·s/m |
| spring-damper (PR11 – PR18) | Stiffness $2.9 \times 10^9$ N/m |
| spring-damper (PR11 – PR18) | damping coefficient $2.207 \times 10^5$ N·s/m |

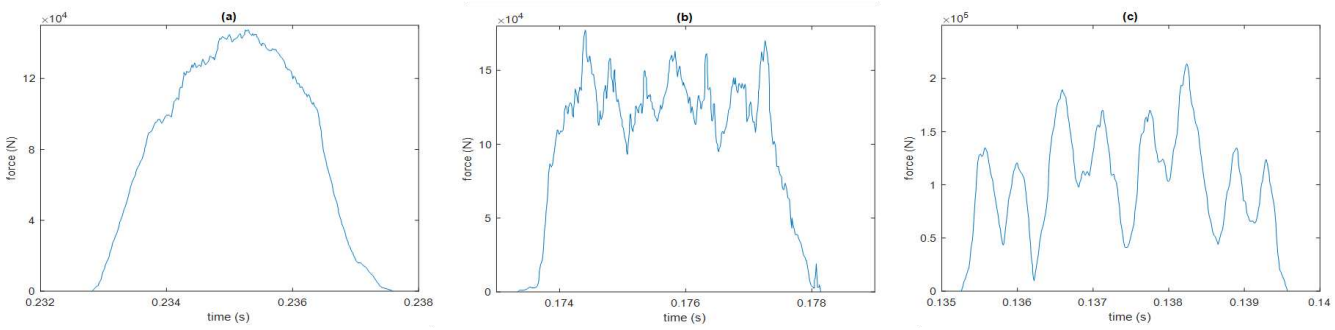



Fig. 5. Dynamic load from the wheel-rail contact at train speeds of (a) 40 km/h, (b) 60 km/h, and (c) 90 km/h

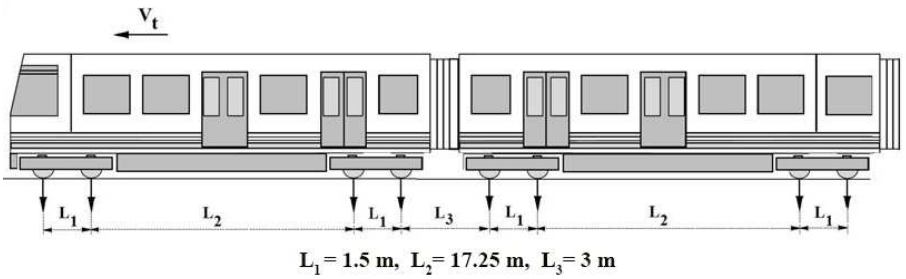



Fig. 6. Schematic illustration of the train wagon

## 2.2 Description of the studied tunnel

This research centers on the Tehran Metro Line 6 project, which traverses a diverse array of urban environments, including densely populated districts, major intersections, arterial roads, and key highways throughout Tehran. The tunnel section under investigation features a circular cross-section, with an inner diameter of 8.15 meters and an outer diameter of 8.85 meters. Each tunnel segment measures 1.5 meters in length and has a thickness of 35 centimeters.

As illustrated in Fig. 8, the surrounding ground is categorized into two distinct zones: the saturated zone and the unsaturated zone. These classifications are essential for accurately modeling soil–structure interaction and vibration propagation. The input parameters used for the numerical model are detailed in Table 4 and Table 5.

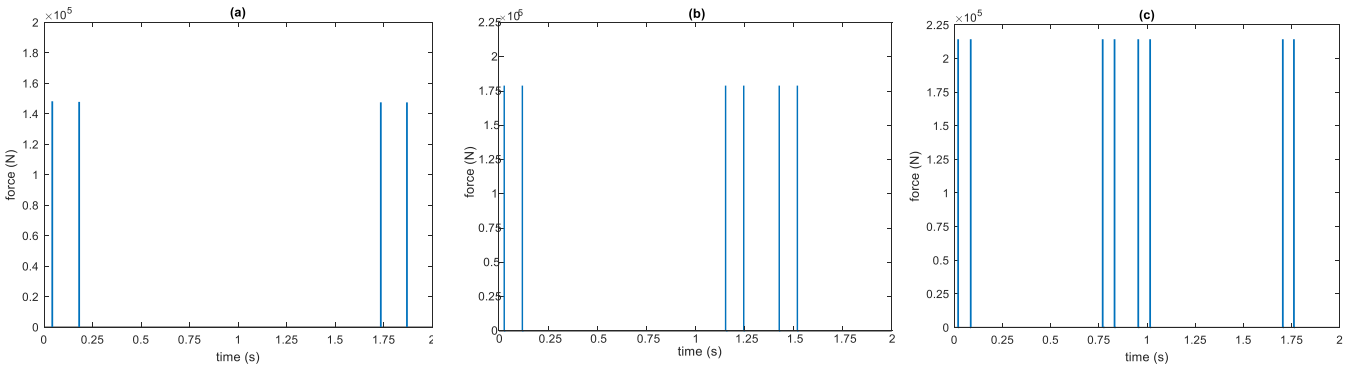



Fig. 7. Final dynamic force at a speed of (a) 40 km/h, (b) 60 km/h, and (c) 90 km/h

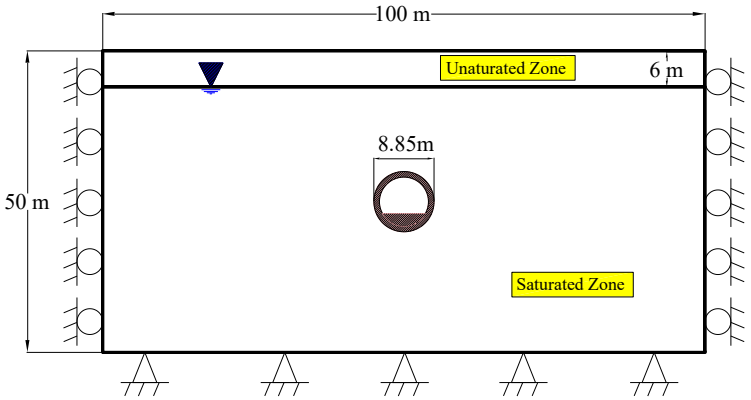



Fig. 8. Dimensions and boundary conditions of the 2D model

Based on the geological profile and longitudinal section of Tehran Metro Line 6, along with insights from prior studies and project-specific data, the Mohr-Coulomb constitutive model was adopted to simulate soil behavior. This model effectively captures the shear strength characteristics of the surrounding ground, making it suitable for tunnel–soil interaction analysis.

For the tunnel support system, an elastic material model was employed to represent the behavior of the precast concrete segments. This approach allows for accurate simulation of segmental deformation under dynamic loading conditions. Following the installation of the tunnel lining, the tunnel invert, where the slab track is positioned, was modeled with a vertical height of 2 meters from the tunnel base, reflecting the actual construction geometry.

Table 4. Input parameters for the soil layer in the tunnel area

| Input parameters | Saturated zone | Unsaturated zone |
|---|---|---|
| Density (kg/m³) | 1938 | 1875 |
| Elastic modulus (Pa) | $51.25 \times 10^6$ | $51.25 \times 10^6$ |
| Poisson's ratio | 0.3225 | 0.3225 |
| Cohesion (Pa) | $26.13 \times 10^3$ | $34.13 \times 10^3$ |
| friction angle (degree) | 28 | 32 |

Table 5. Input parameters for the concrete segment

| Input parameters | Concrete segment |
|---|---|
| Density (kg/m³) | 2500 |
| Elastic modulus (Pa) | $35 \times 10^9$ |
| Poisson's ratio | 0.2 |
| Thickness (m) | 0.35 |

## 2.3 Numerical modeling

A schematic representation of the tunnel geometry is provided in Fig. 8. To simulate the dynamic effects of train movement, the train's load is applied as a point load at the rail locations, representing a double-track configuration. Fig. 9 illustrates the schematic spacing between the

rails. The dynamic load used in this study is derived from three-dimensional finite element modeling, specifically at the wheel–rail contact interface. In contrast, the two-dimensional finite element model excludes pavement components, considering only the concrete tunnel invert as the subgrade. This simplification allows for focused analysis of vertical load transmission through the tunnel structure. It is important to note that the applied dynamic load undergoes a multi-stage transmission process: from the wheel to the rail, from the rail to the sleeper, from the sleeper to the slab track, and finally from the slab track to the concrete tunnel invert. Due to the damping and stiffness characteristics of the intermediate track components, the load transmitted to the sleeper differs from the initial wheel–rail contact load. To account for these attenuation effects, a load escalation factor has been applied to the dynamic loads obtained from numerical modeling at each train speed. This adjustment ensures that the transmitted load more accurately reflects the cumulative impact of the train's passage. The escalation factor and corresponding load profiles are presented in Fig. 7.

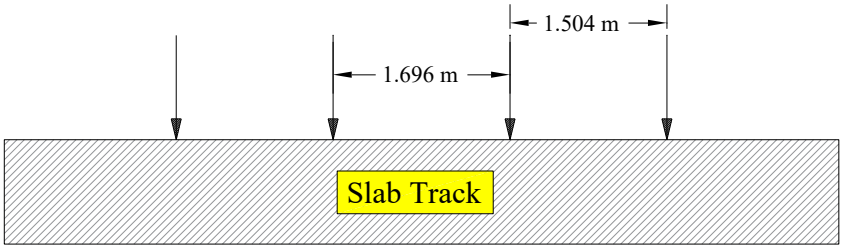



Fig. 9. Schematic representation of the dynamic loads applied to the slab track

In dynamic modeling, it is essential to incorporate the damping characteristics of both the surrounding soil and the structural concrete components. These properties significantly influence the system's response to dynamic loads, particularly in vibration analysis. As shown in Eq. (1), Rayleigh damping is commonly employed to represent the system's overall dynamic damping behavior. This method combines mass- and stiffness-proportional damping, enabling a realistic simulation of energy dissipation across a range of frequencies:

$$M\ddot{u} + C\dot{u} + Ku = F \tag{1}$$

Here, $M$ is the mass matrix, $C$ the damping matrix, $K$ the stiffness matrix, and $F(t)$ the external force vector. The vectors $u$, $\dot{u}$, and $\ddot{u}$ represent displacement, velocity, and acceleration, respectively, as functions of time.

Determining the damping matrix $C$ requires parameters that are often difficult to obtain experimentally. In finite element modeling, it is common to express $C$ as a linear combination of the mass and stiffness matrices, an approach known as Rayleigh damping (Zienkiewicz & Taylor, 1991):

$$C = \alpha M + \beta K \tag{2}$$

In Eq. (2), $\alpha$ governs the mass-proportional damping, while $\beta$ controls the stiffness-proportional damping. The relationship between the damping ratio $\xi$ and Rayleigh coefficients $\alpha$ and $\beta$ is given by:

$$\alpha + \beta\omega^2 = 2\omega\xi \tag{3}$$

where $\omega$ is the angular frequency. Solving Eq. (3) for two distinct frequencies and their corresponding damping ratios yields the Rayleigh coefficients:

$$\alpha = 2\omega_1\omega_2 \frac{\omega_1\xi_2 - \omega_2\xi_1}{{\omega_1}^2 - {\omega_2}^2} \tag{4}$$

$$\beta = 2\frac{\omega_1\xi_1 - \omega_2\xi_2}{{\omega_1}^2 - {\omega_2}^2} \tag{5}$$

To determine the frequencies $\omega_1$ and $\omega_2$, the method proposed by Hudson et al. (1994) and Hashash & Park (2002) is applied. According to this approach, $\omega_1$ is selected as the first natural frequency of the soil mass, while $\omega_2$ is chosen as the nearest whole number greater than the ratio of the dominant input wave frequency to $\omega_1$.

The first natural frequency of the soil mass is calculated using Kramer's method:

$$f_n = \frac{\bar{v}_s}{4H}(2n - 1) \tag{6}$$

where fn is the nth natural frequency, $\bar{v}_s$ is the average shear wave velocity, H is the total thickness of the soil layer, and n is the mode number. Based on Eq. (6), the first natural frequency is determined to be 5 Hz, corresponding to ω1. The dominant frequency of the input vibration wave is obtained via Fourier transform of the dynamic load shown in Fig. 7, yielding ω2.

Assuming a damping ratio of 1%, the Rayleigh damping coefficients α and β are calculated using Eqs. (4)–(5), and the results are presented in Table 6.

Table 6. Frequency and corresponding Rayleigh damping coefficients determined by train speed

| **Speed ($^{km}/_{h}$)** | **$\omega_2$ (Hz)** | **α** | **β** |
|---|---|---|---|
| 40 | 29 | 0.06177 | 0.0001079 |
| 60 | 45 | 0.06214 | 0.00006996 |
| 90 | 101 | 0.06252 | 0.00003136 |

Fig. 10 presents the Rayleigh damping curve derived from the coefficients calculated for a train speed of 40 km/h. A damping ratio of 0.5% is applied to both the tunnel support system and the concrete tunnel invert, reflecting the inherent damping characteristics of concrete materials. To evaluate ground vibration levels, nine distinct scenarios were developed based on the three train

speeds considered in this study: 40, 60, and 90 km/h. These scenarios, illustrated in Fig. 11, encompass various train movement configurations to capture a comprehensive range of dynamic responses. Vibration measurements were conducted at a designated point located at the center of the ground surface directly above the tunnel alignment. Output results were extracted at this location to assess the potential for environmental disturbance caused by underground train operations. The primary objective of this research is to evaluate the extent to which train-induced vibrations along Tehran Metro Line 6 may contribute to surface-level discomfort for residents. This assessment provides critical insights into the environmental implications of underground rail infrastructure in densely populated urban settings.

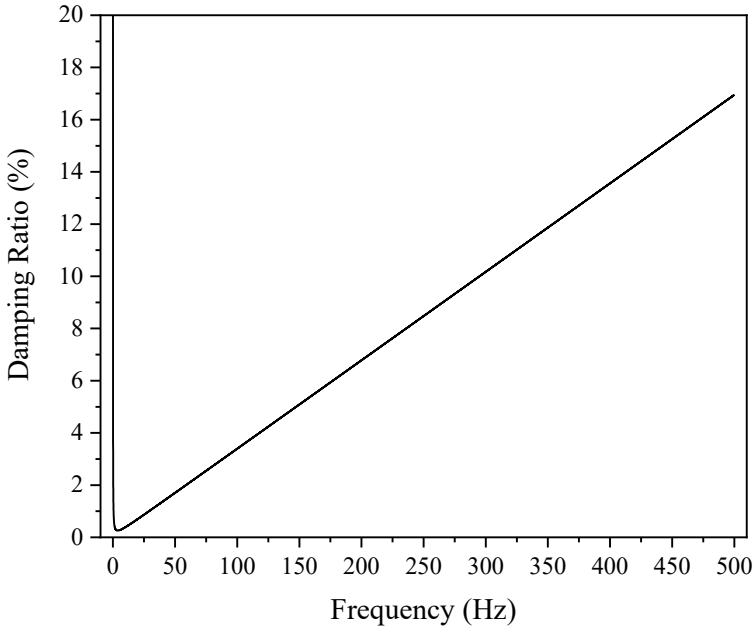



Fig. 10. Rayleigh damping curve using the calculated coefficients

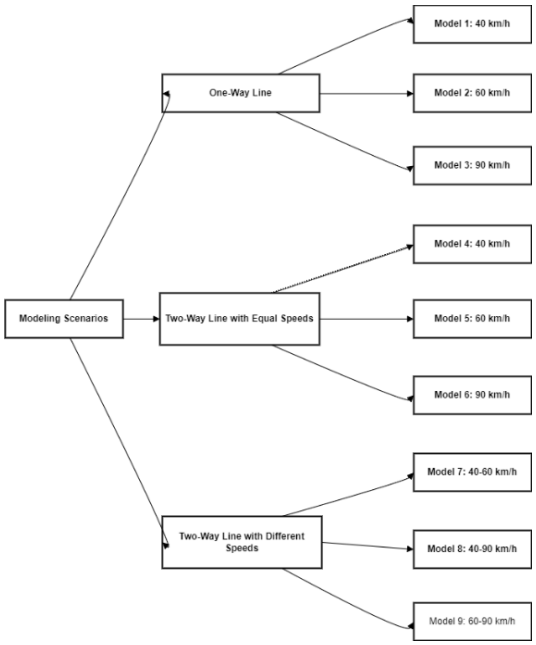



Fig. 11. 9 Scenarios considered for the numerical modeling of vibration levels

To ensure meaningful analysis, the vibration levels obtained from the numerical model must be compared against established regulatory criteria. In this study, the reference standard is provided by the United States Federal Transit Administration (FTA), as illustrated in Fig. 12. This guideline defines acceptable vibration thresholds for various land uses and sensitivities, enabling assessment of potential environmental disturbances. To facilitate comparison with the FTA criteria, vibration levels are expressed in decibel units. The vibration velocity level, denoted as VdB, is calculated using Eq. (7):

.

$$L_v = 20\log(\frac{v_{rms}}{v_{ref}}) \tag{7}$$

where $V_{rms}$ is the root mean square (RMS) vibration velocity in mm/s, and $V_{ref}$ is the reference velocity, typically taken as $10^{-6}$ mm/s. This logarithmic transformation allows for direct comparison with the FTA's decibel-based thresholds. In this equation, $L_v$ represents the vibration velocity level in decibels, $v_{rms}$ is the root mean square of the velocity magnitude and $v_{ref}$ is the reference velocity. According to the FTA, the reference velocity in the U.S. is $1 \times 10^{-6}$ inches per second, while internationally, it is $1 \times 10^{-6}$ meters per second. The root mean square of the velocity magnitude can also be determined using Eq. (8).

$$\mathrm{v_{rms}} = \sqrt{\frac{\sum \mathrm{v_i^2}}{\mathrm{n}}} \tag{8}$$

Where $v_i$ represents the velocity measured through modeling at the selected point over time, and $n$ is the number of data points recorded during that time.

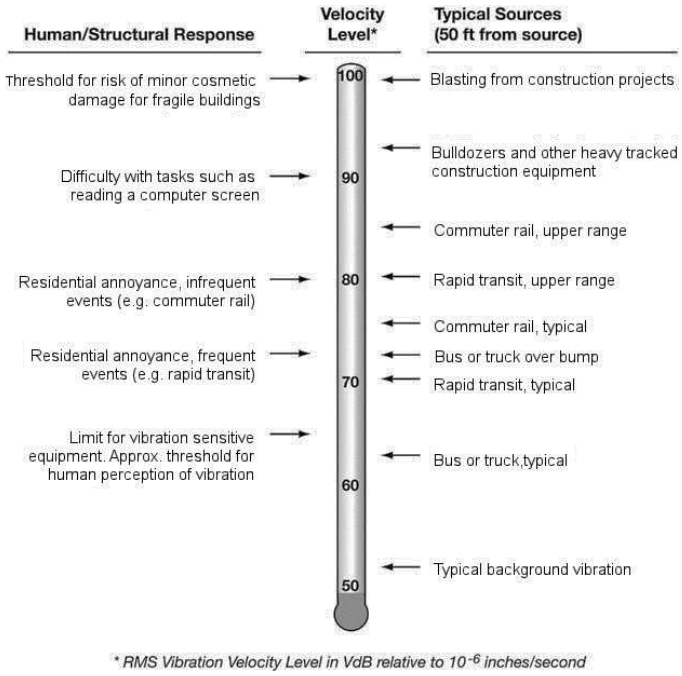



Fig. 12. Ground vibration levels in decibel units (Quagliata, Ahearn et al. 2018)

## 3. Result and discussion

Following the incorporation of the specified parameters during the dynamic force application stage, the refined dynamic model was solved over a 5-second simulation period. The computed results for Scenarios 1 and 6 are illustrated in Fig. 13, providing insight into the temporal evolution of vibration velocity under varying conditions.

As shown in Fig. 12, the acceptable vibration velocity levels for fast rail transport lines are defined by two thresholds: a normal limit of 70 decibels and an upper limit of 80 decibels. These benchmarks serve as critical reference points for evaluating the impact of dynamic loads on surrounding infrastructure and human comfort.

Using Eq. (7), the vibration velocity levels for all nine scenarios were calculated. The corresponding results, including both the decibel values and the peak particle velocities (PPVs), are summarized in Table 7. This comparative analysis enables a comprehensive assessment of each scenario's compliance with established vibration criteria.

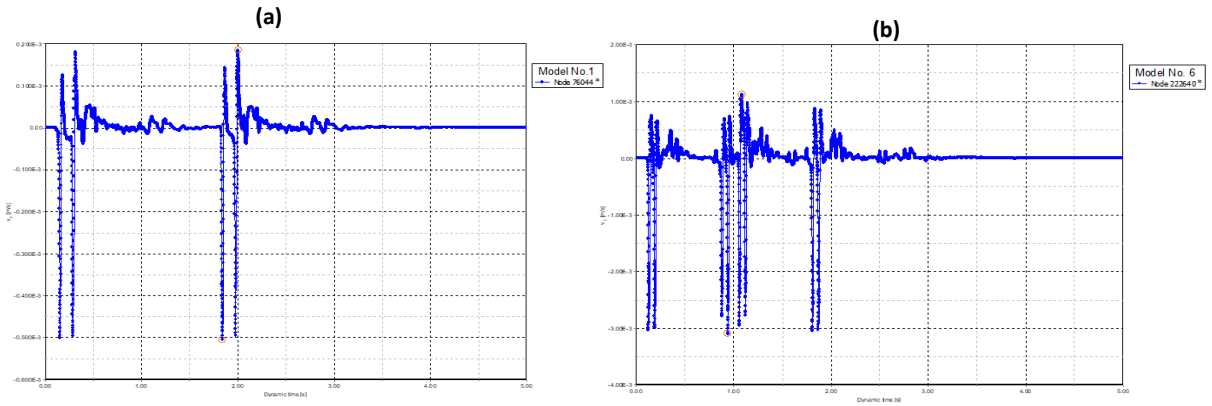



Fig. 13. results for scenario (a) number 1 and (b) number 6

Table 7. Results of the calculated vibration levels and peak particle velocity

| Model number | velocity levels (dB) | peak particle velocity (mm/s) |
|---|---|---|
| 1 | 66 | 0.5 |
| 2 | 74 | 1.22 |
| 3 | 78 | 1.55 |
| 4 | 72 | 1.01 |
| 5 | 80 | 2.43 |
| 6 | 84 | 3.1 |
| 7 | 75 | 1.17 |
| 8 | 77 | 1.27 |
| 9 | 79 | 2.16 |

Numerical modeling results and analysis reveal that the peak particle velocity on the ground surface increases with train speed, particularly between 40 and 60 km/h, as shown in Fig. 14.

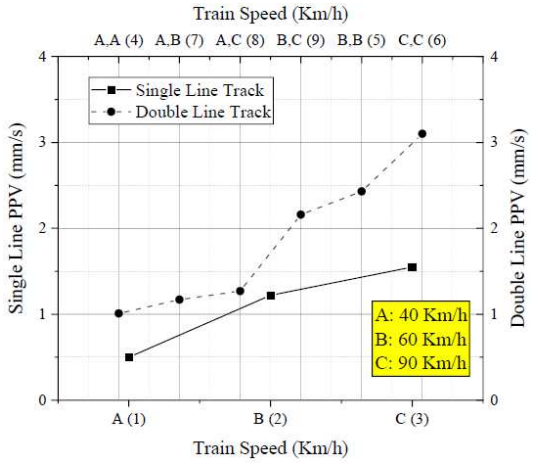



Fig. 14. Comparison of the results for the peak particle velocity

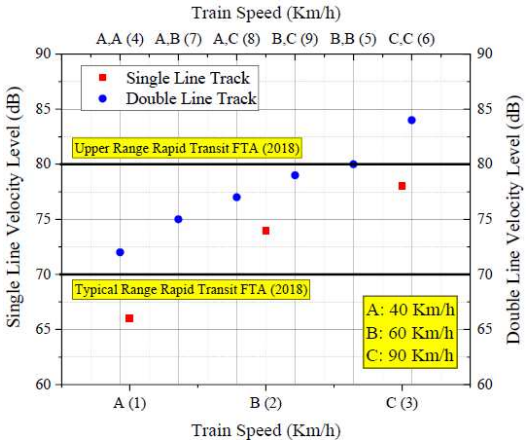



Fig. 15. Comparison of the results for the velocity level

In Fig. 15, the velocity levels obtained through numerical modeling for each scenario in Table 7 are compared with the FTA criteria, as shown in Fig. 12.

As shown in Fig. 15 of the 9 scenarios analyzed, only scenario one (a single track at 40 kilometers per hour) resulted in velocity levels below the normal threshold of 70 dB, while all other scenarios exceeded this level. Additionally, of the 9 scenarios, scenario number 5 (a double track at 60 km/h) and scenario number 6 (a double track at 90 km/h) exceed the upper limit of the specified standard, set at 80 dB. The velocity levels in the remaining scenarios range from 72 to 79 dB. According to the established standard, at the lower end of this range, frequent vibrations may cause discomfort for nearby residents, while at the higher end, even infrequent vibrations can lead to significant disturbances.

## 4. Conclusion

This study systematically investigated the influence of train speed and multi-train interactions on ground-borne vibrations and peak particle velocity (PPV) in soil. The results demonstrate that increasing train speed intensifies the dynamic wheel–rail forces, which in turn elevate ground surface vibrations and PPV. However, this increase is nonlinear. A more noticeable rise in vibration was observed between 40 and 60 km/h, while the increment from 60 to 90 km/h was comparatively moderate. This behavior suggests that at higher speeds, soil damping and the dynamic response of the track ground system mitigate further amplification of vibration levels.

The analysis also revealed that simultaneous passage of two trains significantly increases vibration levels compared to single-train scenarios. The most critical case was Scenario 6, where two trains traveling at 90 km/h generated a maximum vibration of 84 dB and a PPV of 3.1 mm/s. This amplification is attributed to the in-phase superposition of dynamic waves, which enhances constructive interference. In contrast, Scenario 9, involving trains at different speeds (60 and 90 km/h), produced lower vibration levels (79 dB), due to partial wave desynchronization that reduces interference effects. Similar attenuation trends were observed in other mixed-speed scenarios (Scenarios 7 and 8), reinforcing the role of speed mismatch in vibration mitigation.

Compared to FTA standards, vibration levels at 40 km/h remained within acceptable limits. However, at higher speeds, particularly in two-train equal-speed cases, vibrations exceeded permissible thresholds. These elevated levels can disturb nearby residents and interfere with sensitive equipment.

**Funding**

No funding was received for this research.

**Declaration of Generative AI and AI-assisted technologies statement**

This paper was edited with the assistance of Microsoft Copilot, an AI tool used solely for language refinement and sentence restructuring. The authors subsequently reviewed and revised the content as necessary and assume full responsibility for the final publication.

**Declaration of competing interest statement**

This research did not receive any specific grant from funding agencies in the public, commercial, or not-for-profit sectors.

**Data Availability Statement**

All data generated or analyzed during this study are included in this published article.

**References**

Aggestam, E., Andersson, A., & Nielsen, J. C. O. (2018). Simulation of vertical dynamic vehicle–track interaction using a two-dimensional slab track model. Vehicle System Dynamics, 56(11), 1633–1657. https://doi.org/10.1080/00423114.2018.1439573

Ahmadi, M., Nejati, H. R., & Hashemolhosseini, H. (2012). Numerical analysis of ground surface vibration induced by underground train movement. Tunnelling and Underground Space Technology, 29, 1–9. https://doi.org/10.1016/j.tust.2011.12.006

Nejati, H. R., Ahmadi, M., Hashemolhosseini, H., & Hayati, M. (2012). Probabilistic analysis of ground surface vibration due to train movement: A case study on Tehran metro line 4. Geotechnical and Geological Engineering, 30, 1137–1146. https://doi.org/10.1007/s10706-012-9528-z

Anh Dung, T., Van Tuan, N., & Van Duc, N. (2020). Numerical and experimental study of the dynamic factor of the dynamic load on the urban railway. Journal of the Mechanical Behavior of Materials, 29(1), 195–202.

Dai, C., Zhang, Y., & Liu, Y. (2021). Analysis of three-dimensional vibration characteristics of single-circle double-track subway tunnel under moving load. Mathematical Problems in Engineering, 2021, Article 6620301. https://doi.org/10.1155/2021/6620301

Doyle, N. F. (1980). Railway track design: A review of current practice. [Publisher not listed].

Faizan, A. A., Khan, M. A., & Ahmad, S. (2022). Experimental validation of a simplified numerical model to predict train-induced ground vibrations. Computers and Geotechnics, 141, 104547. https://doi.org/10.1016/j.compgeo.2021.104547

Forde, M. C., McCann, D. M., & Clark, M. R. (2017). Evaluating the dynamic behaviour of concrete slab track for high speed rail using numerical analysis. In Railway Engineering–2017 (pp. 1–10). Engineering Technics Press. https://doi.org/10.25084/raileng.22017.20131

Gardien, W., & Stuit, H. (2003). Modelling of soil vibrations from railway tunnels. Journal of Sound and Vibration, 267(3), 605–619. https://doi.org/10.1016/S0022-460X(03)00342-1

Hall, L. (2003). Simulations and analyses of train-induced ground vibrations in finite element models. Soil Dynamics and Earthquake Engineering, 23(5), 403–413. https://doi.org/10.1016/S0267-7261(03)00051-4

Hashash, Y. M. A., & Park, D. (2002). Viscous damping formulation and high frequency motion propagation in non-linear site response analysis. Soil Dynamics and Earthquake Engineering, 22(7), 611–624. https://doi.org/10.1016/S0267-7261(02)00048-2

Heidary, R., Ghasemi, S., & Mohammadi, M. (2021). Effects of train operational parameters on ground-borne vibrations induced by twin metro tunnels. International Journal of Rail Transportation, 9(2), 144–156. https://doi.org/10.1080/23248378.2020.1809316

Huang, Q., Zhang, J., & Liu, Y. (2017). Dynamic response and long-term settlement of a metro tunnel in saturated clay due to moving train load. Soils and Foundations, 57(6), 1059–1075. https://doi.org/10.1016/j.sandf.2017.11.001

Hudson, M. B., Bray, J. D., & Seed, R. B. (1994). QUAD4M: A computer program to evaluate the seismic response of soil structures using finite element procedures and incorporating a compliant base. University of California, Berkeley.

Indraratna, B., Nimbalkar, S., & Christie, D. (2023). Advanced rail geotechnology: Ballasted track. CRC Press.

Jiang, J., Zhang, Y., & Liu, Y. (2020). Dynamic analysis of metro train-monolithic bed track system under tunnel differential settlement. Shock and Vibration, 2020, Article 5632180. https://doi.org/10.1155/2020/5632180

Jin, S. (2016). Resonance response analysis of the slab track caused by moving vehicle. Journal of Vibroengineering, 18(3), 1798–1810.

Li, H., Zhang, Y., & Liu, Y. (2021). Theoretical, numerical, and experimental study on the identification of subway tunnel structural damage based on the moving train dynamic response. Sensors, 21(21), 7197. https://doi.org/10.3390/s21217197

Li, Y., Wang, J., & Liu, Y. (2021). Analysis of dynamic response of subway to adjacent tunnel with different clear distances. Geotechnical and Geological Engineering, 39(7), 5173–5181. https://doi.org/10.1007/s10706-021-01703-6

Ling, L., Zhang, Y., & Liu, Y. (2020). Dynamic interaction between rail vehicles and vibration-attenuating slab tracks. Construction and Building Materials, 258, 119545. https://doi.org/10.1016/j.conbuildmat.2020.119545

Naude, F. P. (2006). Development of a methodology for calculating stresses in track components (Master's thesis). University of Pretoria.

Ntotsios, E., Woodward, P. K., & Laghrouche, O. (2019). A comparison of ground vibration due to ballasted and slab tracks. Transportation Geotechnics, 21, 100256. https://doi.org/10.1016/j.trgeo.2019.100256

Qu, S., Zhang, Y., & Liu, Y. (2021). Experimental study on ground vibration induced by double-line subway trains and road traffic. Transportation Geotechnics, 29, 100564. https://doi.org/10.1016/j.trgeo.2021.100564

Qu, X., Zhang, Y., & Liu, Y. (2020). Dynamic response analysis of the subway station under moving train loads. In Advances in Environmental Vibration and Transportation Geodynamics: Proceedings of ISEV 2018 (pp. 123–134). Springer.

Quagliata, A., & U.S. Department of Transportation. (2018). Transit noise and vibration impact assessment manual. Federal Transit Administration.

Sadeghi, J., & Barati, P. (2010). Evaluation of conventional methods in analysis and design of railway track system. International Journal of Civil Engineering, 8(1), 44–56.

Sadeghi, J., Barati, P., & Askarinejad, H. (2016). Dynamic interaction of vehicle and discontinuous slab track considering nonlinear Hertz contact model. Journal of Transportation Engineering, 142(4), 04016011. https://doi.org/10.1061/(ASCE)TE.1943-5436.0000826

UIC. (2004). UIC 713R: Design of mono-block concrete sleepers. International Union of Railways.

Vale, C. (2021). Wheel flats in the dynamic behavior of ballasted and slab railway tracks. Applied Sciences, 11(15), 7127. https://doi.org/10.3390/app11157127

Wang, A., Zhang, Y., & Liu, Y. (2020). Response characteristics of cross tunnel lining under dynamic train load. Applied Sciences, 10(12), 4406. https://doi.org/10.3390/app10124406

Wu, L., Zhang, Y., & Liu, Y. (2021). Comparison of dynamic characteristics between small and super-large diameter cross-river twin tunnels under train vibration. Applied Sciences, 11(16), 7577. https://doi.org/10.3390/app11167577

Xu, Q.-Y., Zhang, Y., & Liu, Y. (2015). Influence of slab length on dynamic characteristics of subway train–steel spring floating slab track–tunnel coupled system. *Latin American Journal of

Zhu, S., Zhang, Y., & Liu, Y. (2020). Mechanical characteristic variation of ballastless track in high-speed railway: Effect of train–track interaction and environment loads. Railway Engineering Science, 28, 408–423. https://doi.org/10.1007/s40534-020-00210-3

Zienkiewicz, O. C., & Taylor, R. L. (1991). Solid and fluid mechanics dynamics and non-linearity. McGraw-Hill.